A&A 650, A159 (2021)
https://doi.org/10.1051/0004-6361/202040204

Astronomy & Astrophysics

Luminous efficiency based on FRIPON meteors and limitations of ablation models

E. Drolshagen[1,⋆], T. Ott[1,⋆], D. Koschny[2,3], G. Drolshagen[1], J. Vaubaillon[4], F. Colas[4], B. Zanda[5,4,6], S. Bouley[7,4,6], S. Jeanne[4,6], A. Malgoyre[8,6], M. Birlan[4,6,11], P. Vernazza[9,6], D. Gardiol[10], D. A. Nedelcu[11,12], J. Rowe[13], M. Forcier[14,15], J. M. Trigo-Rodriguez[16,17,18], E. Peña-Asensio[17], H. Lamy[19,20], L. Ferrière[21,22], D. Barghini[10,23], A. Carbognani[24], M. Di Martino[10], S. Rasetti[10], G. B. Valsecchi[25,26], C. A. Volpicelli[10], M. Di Carlo[10], C. Knapic[10], G. Pratesi[10,28], W. Riva[33], G. M. Stirpe[10], S. Zorba[10], O. Hernandez[14,15], A. Grandchamps[14,15], E. Jehin[19,27], M. Jobin[14,15], A. King[13,29], A. Sanchez-Lavega[30,31], A. Toni[32,2], A. Rimola[34], and B. Poppe[1]

(Affiliations can be found after the references)

Received 22 December 2020 / Accepted 1 April 2021

ABSTRACT

Context. In meteor physics, the luminous efficiency τ is used to convert the meteor's magnitude to the corresponding meteoroid's mass. However, a lack of sufficiently accurate verification methods or adequate laboratory tests mean that discussions around this parameter are a subject of controversy.

Aims. In this work, we aim to use meteor data obtained by the Fireball Recovery and InterPlanetary Observation to calculate the luminous efficiencies of the recorded meteors. We also show the limitations of the methods presented herein.

Methods. Deceleration-based formulas were used to calculate the masses of the pre-atmospheric meteoroids. These can in turn be compared to the meteor brightnesses to assess the luminous efficiencies of the recorded objects. Fragmentation of the meteoroids is not considered within this model. Good measurements of the meteor deceleration are required.

Results. We find τ-values, as well as the shape change coefficients, of 294 meteors and fireballs with determined masses in the range of 10^{-6}–100 kg. The derived τ-values have a median of $\tau_{median} = 2.17\%$. Most of them are of the order of 0.1–10%. We present how our values are obtained, compare them with data reported in the literature, and discuss several methods. A dependence of τ on the pre-atmospheric velocity of the meteor, v_e, is noticeable with a relation of $\tau = 0.0023 \cdot v_e^{2.3}$. Furthermore, a dependence of τ on the initial meteoroid mass, M_e, is found with negative linear behaviour in log–log space: $\tau = 0.48 \cdot M_e^{-0.47}$.

Conclusions. The higher luminous efficiency of fast meteors could be explained by the higher amount of energy released. Fast meteoroids produce additional emission lines that radiate more efficiently in specific wavelengths due to the appearance of the so-called second component of higher temperature. Furthermore, the negative dependence of τ on M_e implies that the radiation of smaller meteoroids is more efficient. The results of this study also show the limitations of the ablation-based model for the determination of the luminous efficiency.

Key words. meteorites, meteors, meteoroids – minor planets, asteroids: general – comets: general – techniques: photometric – atmospheric effects – methods: data analysis

1. Introduction

Meteor physics is an old discipline but it is driven by new technology. Moreover, it has received new interest, and current research is producing better and more accurate results. However, most of the findings in meteor physics still have relatively large uncertainties compared to terrestrial research areas. This is mainly due to approximations of some parameters, such as the shape of the meteoroid and its mass, which are unknown for each specific meteor and cannot be measured directly. In addition, both parameters change during the flight through the atmosphere in an unknown and difficult to model way. The composition of the meteoroid and the atmosphere also have to be approximated, as well as some other aspects of the detections themselves, like, for example, observational biases or measurement uncertainties. Additionally, the meteoroid's speed, its height, and the meteor's brightness are the most important parameters, and they are not error-free since they are determined from measurement data with inherent uncertainties. Moreover, possible fragmentation of the meteoroid along its path could be important for the observed brightness.

Meteors can be observed with various methods; for example, optically, by radar, or by infrasound (see e.g. Brown et al. 2013 or Ott et al. 2020). The observation equipment determines the meteoroid size range to be recorded. With a small field of view (FOV), high-resolution imaging usually goes hand in hand with many rather faint meteors. Since bright fireballs (visual magnitude mag < −4) are relatively rare, a large FOV is helpful to capture them. However, the larger field of view usually comes at the expense of the resolution of the images. A wide FOV together with a favourable spacing between network nodes allows the detection of bright, rare fireballs from more stations than just one. This makes scientific analyses of quite good quality possible. There are different meteor and fireball networks spread around the world. Meteor networks include projects such as the Spanish meteor network (SPN; Trigo-Rodríguez et al. 2004, 2006), the Slovak video meteor network (Toth et al. 2012), or the Canadian automated meteor observatory (CAMO; Weryk et al. 2013; Weryk & Brown 2013) and fireball networks such as the

⋆ These authors contributed equally to this work.

European fireball network (EFN; Oberst et al. 1998), the global fireball observatory (GFO; Devillepoix et al. 2020), or the desert fireball network in Australia (DFN; Howie et al. 2017). The main focus of this paper is on the Fireball Recovery and InterPlanetary Observation (FRIPON). It is a French-based network that covers France entirely, as well as parts of the neighbouring countries, and is currently extending into the rest of Europe. Additional cameras have already been deployed in other countries worldwide. It is designed for fireball detection and meteorite recovery, consisting of all-sky cameras, see Colas et al. (2020).

One goal of many meteor or fireball observations is to compute, together with the trajectory, the pre-atmospheric mass of the corresponding meteoroid. It is usually one of the main parameters to be determined. To do so, the connection between the entering body's brightness, velocity, and mass is often used. This analysis is in turn based on photometric formulae. To compute the pre-atmospheric meteoroid mass from the meteor's brightness, one has to assume, or ideally determine, what fraction of the loss of kinetic-energy of the object is converted into its brightness. This is described by the parameter τ, that is, the luminous efficiency. The value of τ is part of various studies as it is a very important parameter in meteor research. Different methods to derive the luminous efficiency have been applied and published in, for example, Verniani (1965), Ceplecha & McCrosky (1976), Halliday et al. (1996), Hill et al. (2005), and Weryk & Brown (2013). These studies all found a dependency of the luminous efficiency on the velocity of the impacting object. Overviews are given, for example, in Koschny et al. (2017) and Subasinghe et al. (2017). Even small variations in the value for τ can yield very different results for the meteoroid's mass as shown in the two studies just mentioned. This is especially frustrating as the determination of τ is usually dependent on several assumptions for unknown parameters.

Overall, the conversion between the brightness of a recorded meteor or fireball to the mass of the corresponding meteoroid based on a photometry formula is a complex topic involving multiple dependencies and parameters. Many authors have already addressed this problem in various publications, using different assumptions. In most cases, the brightness of the meteor is integrated along its visible trajectory. The amount of kinetic energy released by deceleration of the entering object in the Earth's atmosphere and which is converted into visible radiation and emitted as luminosity, I, must be estimated. This fraction is the luminous efficiency τ.

Following, for example, Ceplecha et al. (1998), the fraction of the kinetic energy E of the entering object that is radiated can be described as follows:

$$I = -\tau \cdot \frac{\mathrm{d}E}{\mathrm{d}t}. \tag{1}$$

Hence, the luminosity is related to the energy as stated in Eq. (1). The pre-atmospheric meteoroid mass M_e can be computed as

$$M_\mathrm{e} = \frac{2}{\tau \cdot v_\mathrm{e}^2} \int I_\mathrm{s}\, \mathrm{d}s, \tag{2}$$

with the term $\int I_\mathrm{s}\, \mathrm{d}s$ giving the emitted light I in Watts, integrated over the complete flight path s (Verniani 1965).

An alternative way to compute the pre-atmospheric mass of the meteoroid is to use the meteor's altitude and its deceleration rate in the atmosphere. This way the mass can be computed regardless of the luminous efficiency. This was done previously, for example, by Gritsevich (2008a).

In the study just mentioned, Gritsevich (2008a) introduces a dimensionless coefficient method with two parameters, α and β, which are the ballistic coefficient and the mass loss coefficient, respectively. The origin of the method is based on the work by Stulov et al. (1995). α and β can be computed using the generally more precisely determined velocity and height information for the meteor event. Computations based on this method have already made some meteorite sample recoveries possible as shown in the case of the Annama meteorite (see e.g. Gritsevich et al. 2014a,b). The link between α and β and a meteoroid's physical characteristics were used by Moreno-Ibáñez et al. (2018, 2020) and Sansom et al. (2019) to estimate such parameters as final height, final mass, and even meteoroid types.

Furthermore, using the α and β method, Gritsevich & Koschny (2011) were able to compute the luminous efficiency with only very few assumptions. In their work, their starting points were the drag and mass loss equations. Considering a change in the meteoroid's velocity and mass during its trajectory and taking the geometrical relation along the path of the meteor into account, they were able to solve the formulas for the meteoroid's dynamical behaviour. The results derived this way are then compared to the drag rate and light curve that were observed for the considered meteor. Afterwards, τ was computed based on this comparison (Gritsevich & Koschny 2011).

In a similar approach, Subasinghe et al. (2017) computed the luminous efficiency for simulated meteors using classical meteor ablation equations. The simulations were performed following the model of Campbell-Brown & Koschny (2004). Subasinghe et al. (2017) discussed the uncertainties of τ by varying the drag coefficient, the meteoroid density, and the shape factor and inferred errors of factors around two for these parameters. In their study, they mention that those parameters were assumed to be constant during the flight through the atmosphere for every simulated meteor. Furthermore, by modelling different masses and velocities of the meteors, they were able to find an uncertainty of a factor of two. The largest deviations were found for the slowest meteors (Subasinghe et al. 2017). In a follow-up publication, Subasinghe & Campbell-Brown (2018) applied the same approach to 15 meteors recorded by CAMO. Characteristics of the network are detailed in, for example, Weryk et al. (2013). The masses used for the simulated meteoroids were of the order of 10^{-6}–10^{-4} kg (Subasinghe et al. 2017) and the recorded events had masses in the same size range. They studied small and non-iron meteoroids. They found luminous efficiencies for the non-fragmenting meteoroids in the range of 10^{-2}–10^{2}% and a weak relationship between the luminous efficiency and the initial meteoroid mass. A comparison with previously published studies placed their τ-values more in the lower value range, but they also show large scattering. However, only 12 meteors were taken into consideration in their study, with the limitations that such a small data set incurs (Subasinghe & Campbell-Brown 2018).

Similar results were found by Čapek et al. (2019), who investigated double station video observations. In their study, they report on the observation and modelling of the light curves of 53 meteors produced by small iron meteoroids. Hence, they focused on faint, slow, and low-altitude meteors. They found no obvious relationship between the luminous efficiency and the initial velocity of the meteor, and only a weak relationship between the luminous efficiency and the initial meteoroid mass, with similar behaviour to that reported in Subasinghe & Campbell-Brown (2018).

It is also obvious that inferring the luminous efficiency of small meteoroids poses an intrinsic challenge since they exhibit compositional differences (Trigo-Rodríguez et al. 2003). As

stream meteoroids are produced by the decay of undifferentiated asteroids and comets, they are composed of fine-grained aggregates (probably similar to interplanetary dust particles, IDPs) that are built by diverse minerals. The random distribution of such mixtures might produce different bulk chemical compositions and tensile strengths (Rietmeijer 2004; Trigo-Rodríguez & Blum 2009). As a consequence, the meteor ablation columns could have varying chemical elements to be excited during the meteor ablation, so it should produce significant luminous efficiency differences (Borovička & Spurný 1996; Trigo-Rodríguez et al. 2003). Moderately volatile elements are depleted at higher altitudes where excitation potentials are lower, producing the so-called differential ablation (Trigo-Rodríguez et al. 2004; Gómez-Martín et al. 2017). At the same time, faster meteoroids develop a second spectral component that increases the luminosity of their meteors (Borovička 1994; Trigo-Rodríguez et al. 2003). To better understand the changes in luminous efficiency it is important to remember that meteor radiation is not continuous but produced by emission lines that lie in different regions of the electromagnetic spectrum. Just as an example, fast meteoroids containing silicates will show the ionised Si II lines at 408 nm and 635 nm, this way increasing the luminous efficiency (Trigo-Rodríguez 2019). Silicon is a very common chemical element as it forms part of the omnipresent silicates in chondritic materials (Trigo-Rodríguez et al. 2019).

In order to calculate the pre-atmospheric meteoroid mass, historically a value for τ has to be assumed. The value for τ is difficult to determine since it depends on parameters that are usually unknown for a specific meteor and cannot be measured directly. Hence, they have to be estimated with quite some uncertainty.

Several authors have studied the luminous efficiency (Verniani 1965; Ceplecha & McCrosky 1976; Friichtenicht et al. 1968; Ayers 1970; Halliday et al. 1981, 1996; Hill et al. 2005; Weryk & Brown 2013; Gritsevich & Koschny 2011; Nemtchinov et al. 1997; Svetsov & Shuvalov 2018, 2019; Svettsov et al. 2018; Ceplecha & ReVelle 2005; Brown et al. 2013; Subasinghe & Campbell-Brown 2018; Čapek et al. 2019) and published its relation to, for example, the meteor's velocity. Since different assumptions were required depending on the method used in these studies, a direct comparison is difficult. Several factors have to be considered.

The recorded light curve is highly dependent on the detecting instrument used and its interpretation of the assumed blackbody source function. Furthermore, the spectral sensitivity of the instrument affects the received photon radiant power. As the spectra of meteors are not homogeneous (especially since there are various discrete emission lines present), the wavelength sensitivity of the recording instrument influences the detection capability and probability. Borovička et al. (1999) showed a continuum for video meteors as well as diverse differences in emissions of the analysed meteors. Additionally, the assumed composition of the object that caused the observed meteor has a large effect on τ, as shown by, for example, Svetsov & Shuvalov (2018).

Moreover, most studies do not take fragmenting meteoroids into account, even though it is known that fragmentation can have a large influence on the luminosity, as shown, for example, by Subasinghe & Campbell-Brown (2018) and Ceplecha & ReVelle (2005). In fact, most meteoroids are expected to fragment (e.g. Subasinghe et al. 2016).

Abrupt meteoroid fragmentation can occur anywhere along the trajectory, and such behaviour can lead to a sudden increase in luminosity. It is usually observed in cometary aggregates that break apart when the loading hydrodynamic pressure reaches the disruptive strength of the particles. It was used by Trigo-Rodríguez & Llrca (2006, 2007) to infer the intrinsic strength differences of meteoroids from different parent bodies. The meteoroid break-up during the phase of heavy ablation causes the release of the small grains and the vaporisation of volatile species that quickly impulse micron-sized dust to the shock front. As a consequence, large (mm to cm-sized) cometary aggregates often end in a bright flare that is far more luminous than the rest of the ionised column (Trigo-Rodríguez & Blum 2009; Trigo-Rodríguez et al. 2003, 2013). Obviously, this effect should be considered to avoid luminous efficiency overestimation during bright-ending flares.

An overview of the studies referred to and used values for the luminous efficiency is given in Table 1, highlighting the large range of τ-values in current literature. For this work, we calculated τ in an alternative way to show its variability.

This work focusses on the luminous efficiency computation using a deceleration-based method following the procedure of Gritsevich & Koschny (2011), described in detail below in Sect. 3. For the events observed by FRIPON, data are presented in Sect. 2, whereas the computation of luminous efficiencies is presented in Sect. 4. The results are shown in Sect. 5, compared to those from other studies, and relations between the luminous efficiencies and the objects' initial masses and velocities, as well as entry angles, are investigated and presented. In Sect. 6, possible uncertainties and model limitations are discussed, followed by a conclusion.

2. FRIPON data

The Fireball Recovery and InterPlanetary Observation (FRIPON) is a global fireball network launched in France in 2016. These days, it not only covers France, but also several of the neighbouring European countries, and it is expanding worldwide. Consisting of all-sky cameras, it is optimised for fireball detection and meteorite recovery. The stations have an average distance from each other of around 80 km, to allow triangulation measurements of the recorded events. An event that is observed by at least two stations is detected automatically and stored in the FRIPON database. As of May 2020, the network consists of 150 cameras and 20 radio antennas, supplementing the optical observations. The total covered area is about 1.5×10^6 km^2 (Colas et al. 2020). For more details about the network, its distribution, and the collaborating countries, we refer the reader to Colas et al. (2020). The software used for the control of the camera and meteor event detection is called FreeTure (see Audureau et al. 2014 for details).

The station's design is quite simple, which is one of the advantages of the network, opening it up to institutions and amateurs alike. The digital cameras used are DMK 23G445 cameras (Anghel et al. 2019) based on the Sony chip ICX445 with 1.2 megapixels and a pixel size of 3.75 µm × 3.75 µm (Colas et al. 2014, 2020). For now, they only operate during the night with 30 frames per second, and they take one 5-s exposure every 10 min for calibration purposes. The fish-eye lens has a $f = 1{:}25$ mm (Jeanne et al. 2019). Furthermore, FRIPON uses a hardware configuration of a next unit of computing (NUC) with i3 processor, 8 Gb of random-access memory (RAM, for image buffering), 32 Gb solid-state-drive (SSD) for system installation, 1 Tb hard disk drive (HDD), GigE vision, and power over Ethernet (PoE) (Colas et al. 2014, 2020). Since the system has been further developed over the past few years, more recent stations may have a slightly different hardware configuration. For further information about FRIPON, see Colas et al. (2020).

Table 1. Overview of luminous efficiency studies with mass range of the investigated objects, utilised data sources, and derived range of τ-values.

Literature	Mass range	τ range	Sources
Verniani (1965)	Order of 10^{-2} kg	0.02–0.2%	Harvard photographic meteor project, 413 Super-Schmidt meteors, −1 to +0.5 mag
Ceplecha & McCrosky (1976)	10^{-1}–10^{2} kg	0.2–2%	Photographic fireball data, 232 observations, the Prairie networks + laboratory measurements of τ + artificial meteors (Friichtenicht et al. (1968) + Ayers (1970) were taken into account)
Halliday et al. (1996)	10^{-3}–10^{2} kg	1–7%	259 fireballs detected by a Canadian camera network
Hill et al. (2005)	10^{-13}–10^{-6} kg	0.02–0.7%	Numerical, high-velocity meteors
Weryk & Brown (2013)	10^{-8}–10^{-5} kg	0.5–6%	Canadian meteor radar system and optical video camera systems
Gritsevich & Koschny (2011)	1–10^{2} kg	0.6–8%.	Three fireballs of the sample published by Halliday et al. (1996)
Nemtchinov et al. (1997)	0.2–20 m (10–10^{7} kg)	5–10% (bolometric)	Light flashes detected from space by satellites' optical sensors
Svetsov & Shuvalov (2019)	0.3–3 km (10^{10}–10^{13} kg)	1–18% (bolometric)	Simulations
Svetsov & Shuvalov (2018)	30 m and 100 m (10^{7}–10^{9} kg)	2–40% (bolometric) 1–19% (390–775 nm)	Simulations
Brown et al. (2013)	19 m (10^{6} kg)	17% (bolometric)	Chelyabinsk meteoroid
Svettsov et al. (2018)	19 m (10^{6} kg)	17% (bolometric) 6% (350–650 nm)	Chelyabinsk meteoroid
Halliday et al. (1981)	20–40 kg	4–8%	Innisfree meteorite fall from 1977
Subasinghe & Campbell-Brown (2018)	10^{-6}–10^{-4} kg	0.04–1% (some up to 30%)	Small, non-fragmenting and non-iron meteoroids
Čapek et al. (2019)	10^{-6}–10^{-3} kg	0.08–6%	Double station video observations of faint, slow, and low-altitude meteors

Notes. For those works that indicate their size ranges in metres, we estimated the masses in kilograms, assuming a density of 2500 kg m^{-3}. They are stated in parentheses.

Most countries have integrated their national network into the FRIPON database; for example, the Italian network, called PRISMA (Gardiol et al. 2016, 2019), SCAMP in the UK, as well the networks of Germany, the Netherlands, and Spain. Some national networks are still in the installation phase and will also be integrated into the FRIPON database in the future, such as the MOROI network covering Romania (Nedelcu et al. 2018; Anghel et al. 2019).

The data processing in the automated FRIPON pipeline is described in detail in Jeanne et al. (2019). Essentially, an optimisation of a fit through their velocity data is used for astrometrical data reduction. For the photometry the recorded calibration stars' magnitudes were calculated from the computed arbitrary fluxes using star catalogues. With this information, it is possible to compute the absolute magnitudes of the recorded events (the magnitude the event would have if it was detected at the zenith at a height of 100 km), by taking the exposure time and the atmospheric absorption into account, including the air mass and the extinction coefficient (Jeanne et al. 2019).

Recently, initial statistics and results of the FRIPON data were published in Colas et al. (2020). Since 2016, around 3700 events have been detected by the network. Taking the increasing number of installed cameras into account, the network observes on average about 1000 events per year, of which 55% were classified as sporadics. The accuracy of the astrometric reduction is estimated to be 1 arcmin, and the velocity values have uncertainties of about 100 m s^{-1}. Furthermore, the accuracy of the photometry is around 0.5 mag. This value is only valid for non-saturated events with an absolute magnitude of −8 at most. Additionally, FRIPON is not fully efficient for events with an absolute magnitude fainter than −5 mag, which corresponds to a detection threshold for the incoming meteoroids of objects with a size of about 1 cm (Colas et al. 2020).

3. Deceleration-based computations

To compute the pre-atmospheric mass of a meteoroid, a photometric relationship is used in most common methods. It is assumed that during the deceleration in the Earth's atmosphere, a certain fraction of the loss of kinetic energy of the meteoroid is converted into its brightness. How large this fraction is, is the subject of extensive studies with varying values for this luminous efficiency. Using these differing values published in literature can lead to results with a large variation in the mass of the corresponding meteoroid, as shown, for example, in Koschny et al. (2017).

For each recorded event, we have some event-specific parameters, such as, but not limited to, the pre-atmospheric mass and velocity, M_e and v_e, the entry angle γ, and also some calculated values such as the luminous efficiency τ. Some parameters, however, are not only event specific but also time dependent, and they are measured over the course of the trajectory. These parameters include the luminosity I and the velocity v of the meteor. Furthermore, some parameters introduced in the following were divided by the corresponding pre-atmospheric value and are dimensionless; for example the dimensionless velocity v^*. These event parameters are marked with an asterisk.

In an effort to remove the effect of the luminous efficiency on the mass computation, Gritsevich (2008a), along with other authors, developed an approach to compute the pre-atmospheric

mass of the meteoroid by using the altitude of the meteor and its rate of deceleration in the atmosphere. This way, a luminous efficiency does not have to be assumed for its computation. This method is briefly explained here.

Gritsevich (2008a) computed the pre-atmospheric mass of the meteoroid by using the meteor's altitude and the rate of deceleration. This is done by computing the ballistic coefficient α (Eq. (3)) describing the deceleration rate and the mass loss parameter β (Eq. (4)) describing how much mass is lost to the atmosphere (compare Gritsevich 2008a, Eqs. (8) and (9)):

$$\alpha = \frac{c_\mathrm{d} \cdot \rho_0 \cdot h_0 \cdot S_\mathrm{e}}{2 \cdot M_\mathrm{e} \cdot \sin(\gamma)} \tag{3}$$

$$\beta = \frac{(1-\mu) \cdot c_\mathrm{h} \cdot v_\mathrm{e}^2}{2 \cdot c_\mathrm{d} \cdot H}, \tag{4}$$

with the drag coefficient c_d, the atmospheric gas density at sea level ρ_0, the pre-atmospheric cross-section area of the meteoroid S_e, the scale height h_0, the pre-atmospheric meteoroid mass M_e, the angle between horizon and trajectory γ, the heat-transfer coefficient c_h, the pre-atmospheric meteoroid velocity v_e, the effective destruction enthalpy H, and the shape change coefficient μ.

Since α and β are automatically computed by the FRIPON data pipeline (Jeanne et al. 2019; Colas et al. 2020) only a few explanatory details about the method are given in the appendix.

The shape change coefficient represents the effect of the change of the object's shape, ranging from 0 to 2/3. A value of $\mu = 0$ corresponds to the case where the maximal heating and evaporation occurs in the front of the meteoroid, $\mu = 2/3$ represents a uniform mass loss of the meteoroid over the entire surface. Most studies speculate that μ is related to the meteoroid's rotation (e.g. Gritsevich & Koschny 2011 or Sansom et al. 2019).

Using Eq. (5) (Gritsevich 2008a, Eq. (12)), the pre-atmospheric meteoroid mass can be derived. It originated from Eq. (3) converted to M_e with the pre-atmospheric shape factor of the meteoroid A_e and the meteoroid bulk density ρ. In addition to estimates for A_e and c_d, an assumption for ρ is needed. The scale height of the Earth's atmosphere h_0 is expected to be 7160 m, and the gas density at sea level ρ_0 is 1.29 kg m^{-3}:

$$M_\mathrm{e} = \left(\frac{c_\mathrm{d} \cdot A_\mathrm{e} \cdot \rho_0 \cdot h_0}{2 \cdot \alpha \cdot \sin(\gamma) \cdot \rho^{2/3}} \right)^3. \tag{5}$$

Gritsevich & Koschny (2011) used a computation procedure for an event's luminous efficiency depending on the mass and velocity of its source meteoroid, building on the work by Gritsevich (2008a). They derived Eqs. (6) and (7) (their Eqs. (13) and (14)). In these equations, it can be seen that since β and M_e could be derived as explained in Gritsevich (2008a), μ and τ remain the unknown variables in the equations:

$$I(v^*) = \frac{\tau \cdot M_\mathrm{e} \cdot v_\mathrm{e}^3 \cdot \sin(\gamma) \cdot f(v^*)}{2 \cdot h_0}, \tag{6}$$

$$f(v^*) = v^{*3} \cdot \left(\overline{Ei}(\beta) - \overline{Ei}(\beta \cdot v^{*2}) \right) \cdot \left(\frac{\beta \cdot v^{*2}}{1-\mu} + 1 \right) \cdot \exp\left(\frac{\beta \cdot (\mu \cdot v^{*2} - 1)}{1-\mu} \right), \tag{7}$$

with the shape change coefficient μ and the luminous efficiency τ, the exponential integral $\overline{Ei}(x)$,

$$\overline{Ei}(x) = \int_\infty^x \frac{e^z}{z} \mathrm{d}z, \tag{8}$$

and the dimensionless velocity,

$$v^* = \frac{v}{v_\mathrm{e}}. \tag{9}$$

The sole remaining unknown parameter in this equation is the meteor brightness I, which is based on observations. The proper value of μ and τ can then be found by comparing the shape of the observed light curve and applying a least-squares fit with Eq. (6). Hence, μ and τ are derived by finding the best fit of the brightness function to photometrical observations (Gritsevich & Koschny 2011).

To summarise, the specific steps to derive the luminous efficiency of a meteoroid from data of an observed event are the following: first, we obtain α and β from the height-velocity fit calculated by the FRIPON pipeline.

Secondly, we determine the mass M_e according to Eq. (5) with assumptions for A_e, c_d, and ρ.

Then, we obtain the brightness values of the event.

In the last step, we obtain the optimal values of μ and τ from the least-squares fit of the observed light curves and velocities according to Eq. (6).

In Sect. 4, a specific example of the method is presented.

4. Luminous efficiency computation

To illustrate the principle of the computations carried out within the framework of this study, the individual steps are presented in detail below using an example fireball event. The steps carried out are detailed in the summary at the end of Sect. 3.

Table 2 includes some information of the event that occurred on 19 May 2018 around 01:40 UT above the Occitanie region, France. It was detected with seven different stations. It was chosen as an example because the single-station data of the brightness are well suited to visualise the concept. Furthermore, the (calculated) values and properties are close to the average values of the subset analysed herein, and therefore a nice representation of a typical fireball event. An image of the fireball recorded with the FRIPON station located at Onet-le-Château is shown in Fig. 1. The pre-atmospheric velocity of the meteoroid, as computed by the FRIPON pipeline, was 17.2 km s^{-1}. Furthermore, in Table 2 the computed maximum absolute magnitude of the fireball is shown; for a more detailed explanation, please refer to the end of this section. In the last two columns of Table 2, the shape change coefficient μ and the luminous efficiency τ, computed following the method of Gritsevich & Koschny (2011) and described in Sect. 3, are also reported.

4.1. Step 1: Obtain α and β from the height-velocity fit calculated by the FRIPON pipeline

The FRIPON pipeline applies a slightly modified version of the method from Gritsevich (2008a) to compute the pre-atmospheric masses of the meteoroids. The data processing is described in more detail in Jeanne et al. (2019); essentially, an optimisation of a fit through FRIPON velocity data is used. It should be mentioned that for initial onboard data processing purposes, it is assumed that $\mu = 2/3$ from the very beginning. Even though this value of $\mu = 2/3$ is used by most authors in the literature (characteristic for meteoroids with cross-sectional surface areas proportional to their volume to the power of 2/3 and heat redistribution due to rotation to the whole surface), it is an uncertainty that should not be overlooked. Nonetheless, α and β are only based on deceleration data.

Table 2. Details of the 19 May 2018 fireball as detected by FRIPON.

Date	Time (UT)	# Stations	v_e (km s^{-1})	M_e (kg)	α	β	γ (°)	Peak brightness (mag)	μ	τ (%)
2018-05-19	01:40:24	7	17.17 ± 0.03	0.52	77.26	1.21	46.7	–6.7 ± 0.5	0.681 ± 0.003	1.495 ± 0.007

Notes. The table lists: the number of detecting stations, the computed meteor's pre-atmospheric velocity v_e, pre-atmospheric meteoroid mass M_e, the shape change coefficient α, the mass loss parameter β, the slope between horizon and the trajectory γ, as well as the determined maximum absolute magnitude, the shape change coefficient μ, and the luminous efficiency τ derived in this work, as explained in Sect. 2 with Eqs. (6) and (7).

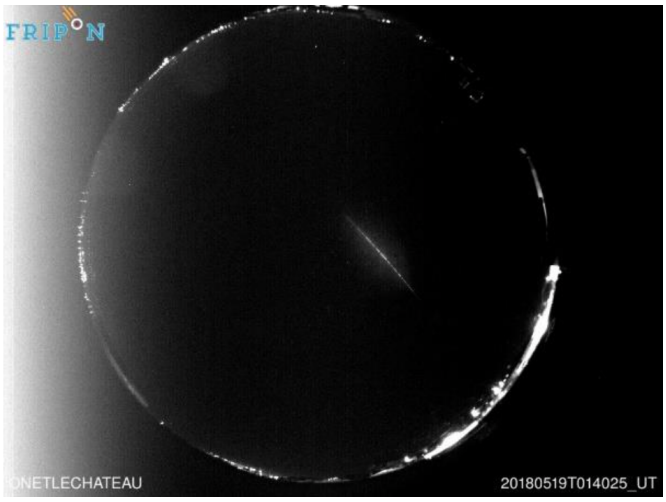

Fig. 1. Fireball from 19 May 2018 as recorded with the FRIPON station Onet-le-Château (Occitanie region, France).

Since we used the Gritsevich & Koschny (2011) method to process the FRIPON data, we are able to apply our own least-squares fit to the observed light curves and find the optimal values of μ and τ. Depending on the assumed values for A_e, c_d, and ρ, and the obtained value of μ, M_e might differ from the values determined by the FRIPON pipeline.

For every event analysed by FRIPON, the following necessary values were extracted: the mass loss parameter β, the pre-atmospheric velocity v_e, and the slope between horizon and trajectory γ. The other event specific parameter from Gritsevich (2008a), the ballistic coefficient α, is also computed and listed but is not required for the computation of the luminous efficiency with the applied method.

4.2. Step 2: Determine the mass M_e according to Eq. (5) with assumptions for A_e, c_d, and ρ

As can be seen from Eq. (6), the pre-atmospheric meteoroid mass M_e is needed to compute τ. M_e is determined with Eq. (5). In this step, some assumptions have to be made. In literature, these assumptions vary from one study to another.

The equation includes the drag coefficient c_d, the pre-atmospheric shape factor of the meteoroid A_e, and the meteoroid bulk density ρ. As in Gritsevich & Koschny (2011), we assumed $c_d = 1.2$ and $A_e = 1.5$. Another common assumption is an initial spherical shape of the meteoroid, with $A_e = 1.21$ and $c_d = 1$. A review of generally used assumptions and parameters can be found in Gritsevich (2008b). Assumed values for the meteoroid bulk density ρ can span a wide range of values, as discussed in Gritsevich & Koschny (2011). The European cooperation for space standardisation (ECSS) supposes a meteoroid density of $\rho = 2500$ kg m^{-3} for impact risk assessments for satellites (ECSS 2008). For about 45% of the whole FRIPON data set, Colas et al. (2020) found a shower affiliation. Hence, we expect that a lot of events originate from cometary material with densities lower than typical meteorites (closer to $\rho = 400$ kg m^{-3}; Sosa & Fernández 2009). As the most fragile parts do not survive their way through the atmosphere, meteorite densities can at most be taken as an upper boundary density for a set of recorded meteoroids. We use the ECSS meteoroid density estimation for the computations in this study.

Nonetheless, all these parameters do affect the mass, and hence the results for the luminous efficiency, too. Thus, the varying assumptions for these parameters from one study to another contribute to a wide range of luminous efficiency values.

Furthermore, the values computed by FRIPON, for example α and β, are not free of errors. For example, to compute the pre-atmospheric meteoroid mass (see Eq. (5)), α is needed. The pre-atmospheric mass is proportional to α by $M_e^3 \propto \alpha$. Furthermore, the brightness is proportional to the pre-atmospheric mass, as can be seen in Eq. (6) and hence to α by $I^3 \propto M_e^3 \propto \alpha$. If one converts the formula to the luminous efficiency, it is also easy to see that $\tau^{-3} \propto M_e^3 \propto \alpha$. Hence, an error in α of a factor of 2 would cause an error in the computations by a factor of 8 in M_e and τ. This emphasises how much the luminous efficiency is dependent on α.

4.3. Step 3: Obtain the brightness values of the event

For each event, the trajectory is computed by the FRIPON pipeline and the object's velocity is calculated taking the underlying station's data quality into account. This is explained in detail in Jeanne et al. (2019). So far, this is only done for the astrometry and not for the photometry. Therefore, the meteor's brightness is only available for an individual station's recorded data.

In order to calculate the luminous efficiency, we combined the calibrated individual stations' brightnesses and the processed trajectory's velocity for the points in time at which the meteor was visible. The single-station brightness is provided in absolute magnitude values. We excluded outliers from these single stations' magnitude data, and if more than 50% of a light curve of any station was excluded, the entire light curve was not considered in further calculations.

In Fig. 2, the interpolated absolute magnitude, single-station data of our example fireball is presented as linestyle-coded lines. The median absolute magnitude values are shown as blue dots and were calculated for each point in time when the fireball was visible. The curve's data points are obtained as follows. First, from all stations' absolute magnitude values, the outliers at each

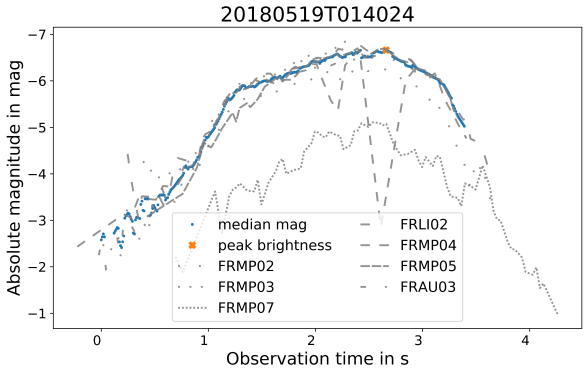

Fig. 2. Interpolated absolute magnitude data from seven single stations for the fireball from 19 May 2018 presented as linestyle-coded lines. The x-axis displays the time of observation of the fireball (in seconds), starting with the time of the first absolute magnitude value from the stations considered (first value of the computed median magnitudes), which correlates with 01:40:25 UT. The median absolute magnitudes, calculated for each point in time the fireball was visible, are shown as blue dots. The maximum brightness of this median curve is highlighted with an orange '×' and is −6.7 mag.

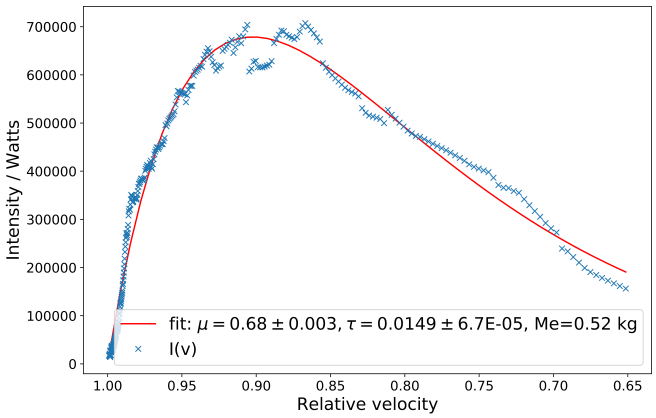

Fig. 3. Computed light curve of the fireball from 19 May 2018 with applied fit. The x-axis displays the relative velocity v^* of the fireball for which each velocity value is divided by the fireball's initial velocity. The brightness values, calculated as explained in Sect. 4.3 for each point in time for which a median magnitude value could be determined, are shown as a blue '×'. The applied fit is displayed as a solid red line.

point in time are excluded by applying the statistical three-sigma rule: all values that do not lie within three standard deviations of the mean value are disregarded (see e.g. Everitt & Skrondal 2002). All single-station data light curves of which more than 50% of the data were rejected were also excluded from further calculations. For all remaining data points, the three-sigma rule is applied again. This way, parts of the curves with large deviations are discarded as well. In Fig. 2, it can be clearly seen that in this way the data of station FRMP07 as well as parts of FRMP04 will be classified as outliers. If data of only one station is available for parts of the observed time frame, this part of the light curve is also rejected. The peak brightness of the resulting median magnitude curve is highlighted in the Fig. 2 with an orange '×' and is listed in Table 2.

Since the luminous efficiency calculation requires the luminosity I, we use our derived median absolute magnitude values Mag as presented as blue dots in Fig. 2 and compute the intensity in Watts with Eq. (10) (compare Eq. (18) in Gritsevich & Koschny 2011, which is based on an equation developed by Ceplecha & ReVelle 2005):

$$I = 10^{-0.4 \cdot \mathrm{Mag} + 3.185}. \tag{10}$$

However, some challenges of this method should be considered: In the case of particularly bright events, the cameras will saturate at around −8 mag. However, only the data of individual stations are affected, particularly those located close to the event. Other stations, further away, should record unsaturated data. The erroneous values should be recognised as outliers during the calculation of the median curve and then ignored for the rest of the calculation. The data set used in this study consists of 24 events with peak brightnesses brighter than −7 mag, and for which we would consider they might be affected by saturation effects. Also to be considered are clouds that could occur and would affect the data of individual cameras. A weighting of the single-station data based on its quality could enhance the accuracy of the magnitude values. However, this could also introduce sources of error due to necessary assumptions. An error of 1 magnitude would lead to a factor of about 2.5 difference in brightness, and hence to a luminous efficiency with the same error (see Eq. (6)). Since the FRIPON cameras are all-sky cameras, the photometric values are expected to have relatively large uncertainties of the order of 0.5 mag. Keeping this in mind, we expect the brightness values computed as explained here to be quite a good compromise between accuracy and computational efforts.

4.4. Step 4: Obtain the optimal values of μ and τ from the least-squares fit of the observed light curves and velocities according to Eq. (6)

For the events in the FRIPON database, the data are extracted and the brightness computed as explained above. Applying a least-squares fit to the light curve, the parameters μ and τ are found as explained in Sect. 3. In Fig. 3, the median light curve with resulting fit is presented for the fireball from 19 May 2018.

The error estimations of the luminous efficiency and the shape change coefficient are based on their respective fits to the light curve. These are purely statistical errors of the fit and do not include other potential measurement errors or uncertainties. Please refer to Jeanne et al. (2019) and Colas et al. (2020) for a discussion on the FRIPON generated parameters' errors.

5. Data, results, and discussion

In Colas et al. (2020), an overview of the FRIPON database and parameters of the recorded events is presented. The status as of 4 July 2020, is that there are 3871 confirmed events in the database. To be confident in our results, a number of quality control steps were taken, eliminating over 90% of these events, resulting in 294 high quality events to analyse.

Initially, only events were selected that had sufficient data to apply the methods presented in this work. For those events, the parameters were extracted and the brightnesses and luminous efficiencies were computed as described in Sect. 4 (see Table 2 for the fireball presented in detail in this work). In total, 1593 of the confirmed events had data sufficient to apply the method presented in this work. The other events were excluded from further calculations. The primary reason to exclude an event is the small number of cameras that detected the event. The method used in this work to calculate the light curve is only possible if at least two cameras have data from overlapping time ranges. This, as well as strong deviations in the individual cameras'

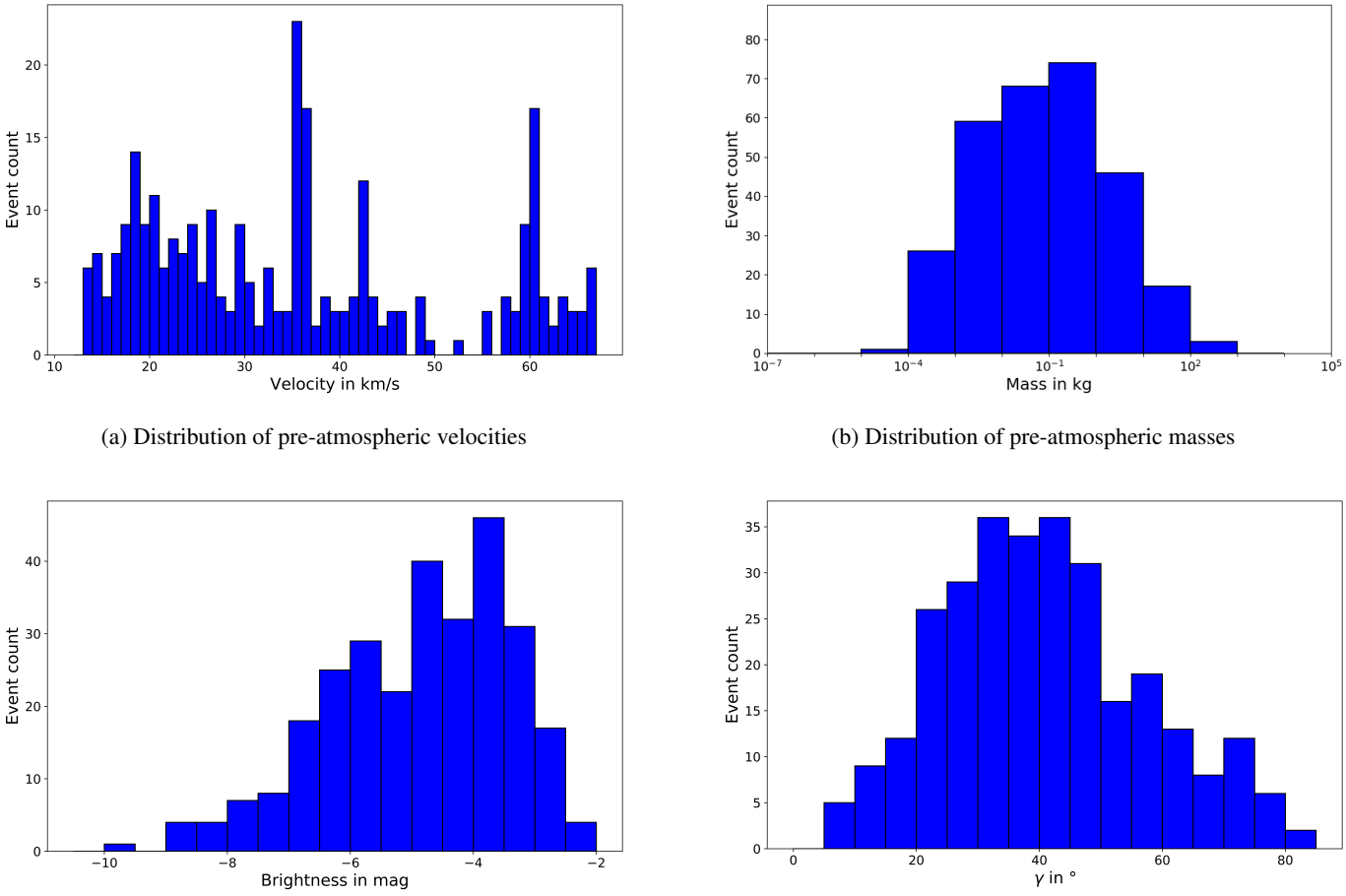

(a) Distribution of pre-atmospheric velocities

(b) Distribution of pre-atmospheric masses

(c) Distribution of peak brightnesses

(d) Distribution of entry angles

Fig. 4. Velocity distribution (*a*), mass distribution (*b*), distribution of peak brightnesses (*c*), and distribution of entry angles (*d*) of the 294 FRIPON events that meet the quality standards set for this study (see text for details) and form our subset.

magnitude data, led to insufficient brightness information for proper evaluations to be achieved. This situation often happens when significant weather differences are noticeable between the observing stations, mostly due to fog, clouds, etc, or when the event is only visible very close to the horizon in an individual station's data.

Of the remaining events, those that produced unrealistic results were also excluded. To do so, all events where best-fit values of τ and μ are outside the realistic range were not included in further calculations. In addition, only those events with light curves allowing a qualitatively good fit were taken. To do this, the relative errors of μ and τ were computed based on the errors from the fitting process. Events with a relative error for τ larger than 0.04, or with a relative error for μ larger than 0.1, were also excluded. Additionally, the remaining events were manually inspected and some with fits that did not match the curve well were also excluded. This mainly concerned events for which only a few data points were available. Hence, the determined error values of the fit parameters were relatively small and the events were not automatically excluded. This way, a total of 294 events with satisfactory parameters and manually confirmed good fits were left of the initial 3871 events that were considered. Thus, less than 10 % of the whole available data set was used for this work. This is emphasised here as we cannot rule out that this introduced a bias in the study. However, it should be mentioned that a bias could be present even within the entire sample. The investigation of possible observational biases should be carried out as part of future studies.

The results presented in Figs. 4–7 are derived quantities for which the calculation is based on different data that are processed in several ways. The velocities and entry angles are automatically calculated by the FRIPON system based on the measured height and position information of the meteor. For the entry mass computation, we used α and β, which were also automatically computed by the FRIPON pipeline based on the deceleration information and some assumptions for unknown parameters such as the meteoroids' densities. The luminous efficiency and the shape change coefficient are derived in this study as described in Sects. 3 and 4.

The meteors considered for this study include sporadic and stream objects. The velocity distribution of these 294 objects is shown in Fig. 4a, and the mass distribution is shown in Fig. 4b. Figure 4a indicates that a large number of the analysed events are related to meteor showers. The peaks of the Perseids in August, with typical velocities of about 59 km s^{-1} and of the Geminids in December, of about 35 km s^{-1} (IMO, 2017) are clearly visible. As mentioned in Colas et al. (2020) around 45% of the recorded events in the FRIPON database are related to meteor showers.

The smallest object in our data set has a pre-atmospheric mass of about 9×10^{-6} kg, the largest one of ca. 32 kg. The median of the masses is $M_{\mathrm{e,median}} = 0.0085$ kg. As mentioned before, due to the different assumptions the mass values

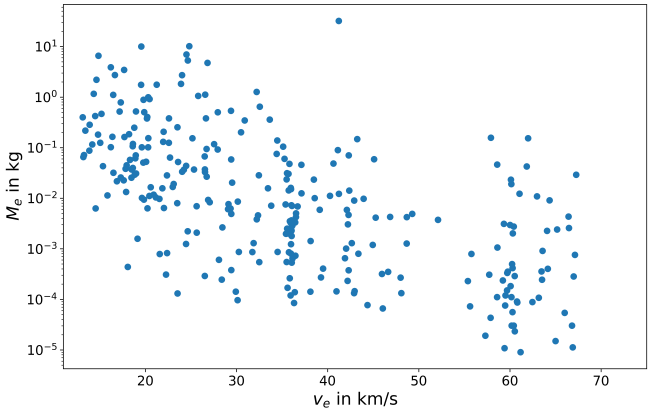

Fig. 5. Masses of the entering objects as a function of their velocities.

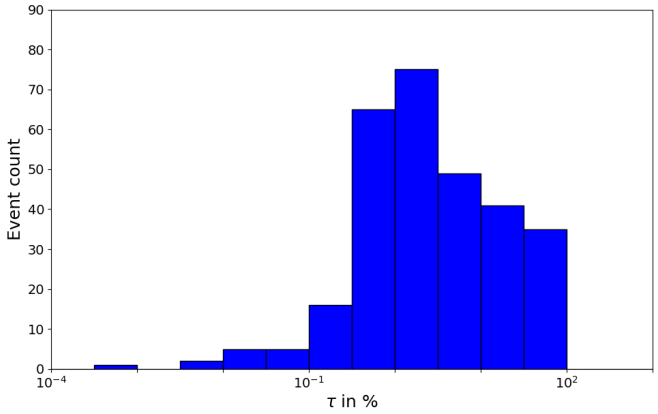

Fig. 6. Distribution of the luminous efficiencies τ derived in this work.

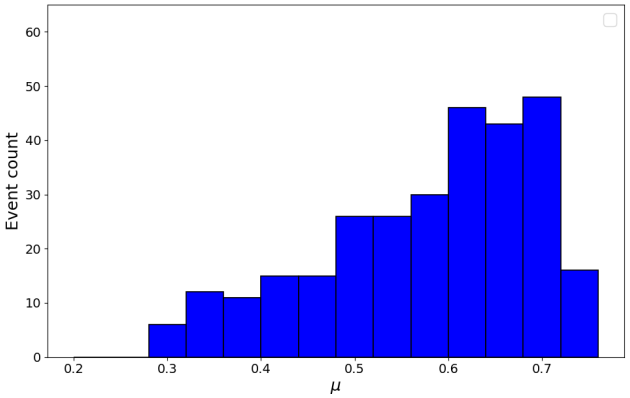

Fig. 7. Distribution of the shape change coefficient μ derived in this work.

presented herein differ from the ones determined by the FRIPON pipeline. For the same density estimate, our values are about half an order of magnitude larger than in Colas et al. (2020). The slowest event has a pre-atmospheric velocity of around 13.1 km s^{-1}, the fastest one of about 67.3 km s^{-1}. The median of the velocities is $v_{\mathrm{e,median}} = 34.8$ km s^{-1}.

The distribution of peak brightnesses is shown in Fig. 4c. The values are the absolute magnitude values computed as described in Sect. 4.

Additionally, the distribution of the objects' entry angles is presented in Fig. 4d. γ describes the angle between the horizon and the trajectory. It is apparent that most meteoroids entered the Earth's atmosphere at an angle between 30° and 50°, and the median value is $\gamma_{\mathrm{median}} = 39.3°$. Since almost 2/3 of the events show $\gamma < 45°$, the majority of them tend to impact at a rather shallow angle.

Figure 5 shows the masses of the entering objects against their velocities. As expected, small objects were only detected if they were fast. This bias has to be kept in mind and should be further considered in future studies.

The distribution of the luminous efficiency τ is shown in Fig. 6 and the distribution of the shape change coefficient μ in Fig. 7. As can be seen, our luminous efficiency values differ by orders of magnitudes ranging from 10^{-4}% up to 100%. Approximately 70% of the τ-values are of the order of 0.1–10%, only about 4% are smaller (between 10^{-4} % and 10^{-1}%), and 26% of the data showed a luminous efficiency in the range of 10–100%. The median of the τ-values is $\tau_{\mathrm{median}} = 2.17$%, and that of the shape change coefficient is $\mu_{\mathrm{median}} = 0.61$.

The calculated values for the luminous efficiency, as presented in Fig. 6, can reach 100%. This is rather surprising and obviously unphysical. This is a first and clear indication that either the observational data is not of sufficient quality or that the applied deceleration model, which is based on ablation, has a limited range of applicability. This is further investigated in the following.

As can be seen in Eqs. (6) and (7), the shape change coefficient μ does significantly affect the form of the light curve. Hence, this parameter is another important topic, besides the question of luminous efficiency, addressed in this paper. A value of $\mu = 0$ corresponds to a case in which only the front of the object ablates, but the cut-through surface area remains constant and only the front hemisphere changes. Hence, the maximal heating and evaporation occurs only in the vicinity of the front critical point of the meteoroid, and the other parts of the body do not change during its journey through the atmosphere. Many studies assume $\mu = 2/3$, including, for example, Halliday et al. (1996) and Jeanne et al. (2019). The case represents a uniform mass loss of the body over the entire surface area. For example, Gritsevich & Koschny (2011) drew a comparison of the shape change coefficient to the rate of the meteoroid's rotation. According to them, a value of $\mu = 0$ corresponds to a case in which the entering object shows a stabilised motion without rotation. In the case of $\mu = 2/3$, the rotation is rapid and chaotic, allowing consideration of a nearly consistent body shape, shrinking uniformly. Equation (6) indicates that the luminous efficiency has less influence on the shape of the light curve and rather influences the height of the intensity peak of the recorded curve, that is, the luminosity of the recorded event. Since τ indicates the percentage of initial kinetic energy that has been converted into light, this is the expected behaviour. This could also point towards a bias in the observations. If only a small part of the energy is converted into visible light, the event might be too faint to detect. Therefore, the distribution of the luminous efficiency presented in this work could underestimate smaller values of τ. The same is valid for other factors in Eq. (6), like the pre-atmospheric meteoroid mass and velocity M_e and v_e, as well as the entry angle γ.

Since μ and τ represent the physical properties of an event, they can be used to exclude unphysical objects from the analysis. Very small values of μ seemed to represent non-working fits to the light curve. Hence, values $\mu < 0.01$ were excluded. Moreover, based on the errors of μ and τ cases with fits that did not work well were excluded. These limit values were found by studying a large number of light curves and applied fits. Cases with relative fitting errors of μ greater than 0.1 or of τ

larger than 0.04 were excluded from the analysis. The relative error is also the basis for our upper limit of μ. A value for μ of 2/3 should be seen as the physical upper limit. In combination to a relative error of less than 0.1 for this value, we accept values of up to $\mu = 0.73$. These limits reduce the number of 'good' events to 294 out of over 1000 events that we were able to analyse.

It is acknowledged that these thresholds were chosen based on subjective interpretations. An even more detailed study of the quality of the fits to the light curves and the light curves themselves could be considered in future work but goes beyond the scope of this study. The given errors of μ and τ are solely based on the statistical quality of the fit. They do not include other uncertainties. Figure B.1 in the appendix shows τ as a function of μ, with fitting errors for both values.

Furthermore, it should be kept in mind that the model of the light curve used does not take fragmentation into account. However, for some events fragmentation is clearly visible in the light curves. Nevertheless, these events were included in this analysis as long as the fit was reasonably good and using the criteria mentioned above. A more detailed analysis of the light curves and possible adjustment of the fit curves represents an interesting aspect for future works. Abrupt meteoroid fragmentation can lead to a sudden increase in luminosity. Such a behaviour can occur anywhere along the trajectory. It is usually observed in cometary aggregates that break apart when the loading hydrodynamic pressure reaches the disruptive strength of the particles (Trigo-Rodríguez & Llrca 2006, 2007). The luminous efficiencies plotted over the events' velocities are presented in Fig. B.2, τ over the events' corresponding meteoroids' masses in Fig. B.3, and τ over the events' entry angles γ in Fig. B.4 in the appendix.

In Fig. B.2, a weak relation between the luminous efficiency and initial velocity of the event can be seen in semi-log space. τ seems to be larger for larger velocities. A relationship between the luminous efficiency and the initial meteoroid mass with negative linear behaviour can be clearly seen in log–log space in Fig. B.3. Furthermore, a weak relation between τ and the entry angle is visible in Fig. B.4. The dependency of τ on the entry angle is only weak, and all relations show a large range of scattering.

A possible dependence of μ on the mass, velocity, and entry angle of the objects was also investigated, but no correlation was found. Furthermore, no dependency of either τ or μ on the peak brightness could be seen.

The objects analysed in the course of this work are in the 10^{-6}–100 kg mass range. Our luminous efficiency values range from 10^{-4}–100%, most are of the order of 0.1–10%. The luminous efficiencies reported in the literature and presented in Table 1 span a wide range of values. They are based on different types of studies of objects of different compositions in various velocity and size ranges. Our derived τ-values are larger than those of most previous meteor and fireball studies dealing with smaller objects, but they are consistent with studies of fireballs and larger asteroids. For the latter, the luminous efficiencies also fell into the 10% range.

Two examples of fireball studies were conducted by Halliday et al. (1996) and Ceplecha & McCrosky (1976). For the larger meteoroids, or even asteroids, their formulas might be more valid. Their values for the luminous efficiencies are of the order of a few percent, and both found a velocity dependency of τ. Since the FRIPON data also consist mainly of fireballs, the results were expected to be most suitable for a comparison. The equations of τ as given in the two works are presented in the appendix and were plotted in Fig. 8, taking the panchromatic response into account.

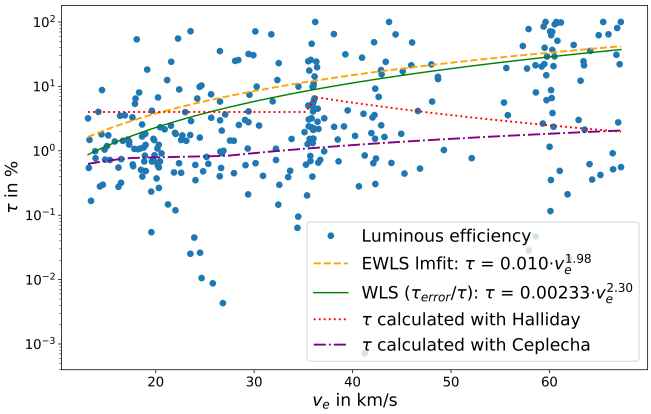

Fig. 8. Luminous efficiency over the initial velocity of the events with fits through the data in semi-log space. Blue dots: values of τ. Orange dashed line: equal-weighted least-squares fit (EWLS) applied to the data. Green line: weighted least-squares fit (WLS) applied to the data; the method weights the values by the relative error of the value. Red dotted line: results found by Halliday et al. (1996). Purple dashed-dotted line: results found by Ceplecha & McCrosky (1976).

To quantify the relation between the luminous efficiency and initial velocity of the event as seen in Fig. B.2, a least-squares fit was utilised to optimise the parameters of the function $\tau = b \cdot v_e^a$. This is presented in Fig. 8 in semi-log space. The equal-weighted least-squares fit (EWLS) gave $b = 0.010 \pm 0.013$ and $a = 1.94 \pm 0.31$, the weighted least-squares fit (WLS) $b = 0.0023 \pm 0.0036$ and $a = 2.30 \pm 0.38$. The WLS method weights the values by the relative error of the luminous efficiency. Due to this, we expect the WLS method to represent the best estimate:

$$\tau = 0.0023 \cdot v_e^{2.3}. \quad (11)$$

In this study, we also tested other fit functions, and the distribution seems to show a quadratic dependence of τ on the velocity. Since the luminous efficiency represents a percentage of the object's energy, this relation seems to be reasonable.

However, it is clear that the relative errors of the fitting parameters are quite large. This should be kept in mind as well as the large scattering the values exhibit (see Fig. 8). Yet, the luminous efficiencies are of comparable orders of magnitude to the literature values.

In the most recently published studies by Subasinghe & Campbell-Brown (2018) and Čapek et al. (2019), a weak relationship between the luminous efficiency and the initial meteoroid mass with negative linear behaviour in log–log space was found. The equations of τ as given in both works are presented in the appendix.

In Fig. 9, the luminous efficiencies are presented as they were derived in this work. They are plotted against the event's mass with a fit through the data in log–log space. Following Čapek et al. (2019), a fit with $\tau = \phi \cdot M_e^{\Omega}$ was applied to our data. EWLS gave $\phi = 0.63 \pm 0.14$ and $\Omega = -0.44 \pm 0.02$, WLS $\phi = 0.48 \pm 0.11$ and $\Omega = -0.47 \pm 0.02$ (with initial mass M_e in kg). Additionally, the results found by Subasinghe & Campbell-Brown (2018) and Čapek et al. (2019) are included in Fig. 9 for comparison.

Again, we expect the WLS method to represent the best estimate:

$$\tau = 0.48 \cdot M_e^{-0.47}. \quad (12)$$

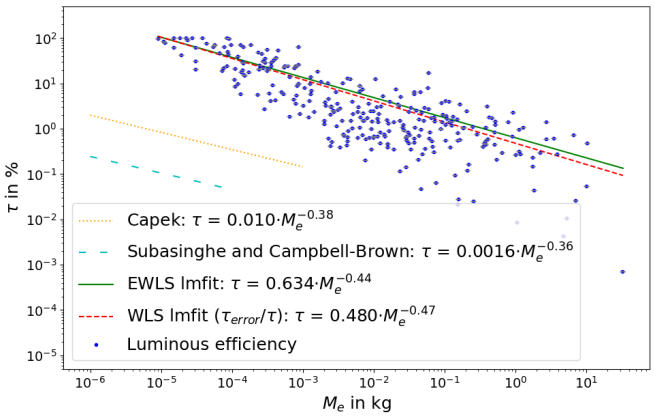

Fig. 9. Luminous efficiencies as derived in this work plotted over the event's corresponding meteoroid's mass with fit through the data in log–log space. Blue dots: values of τ. Green line: equal-weighted least-squares fit (EWLS) applied to the data. Red dashed line: weighted least-squares fit (WLS) applied to the data; the method weights the values by the relative error of the value. Orange dotted line: results found by Čapek et al. (2019). Blue dashed-dotted line: results found by Subasinghe & Campbell-Brown (2018).

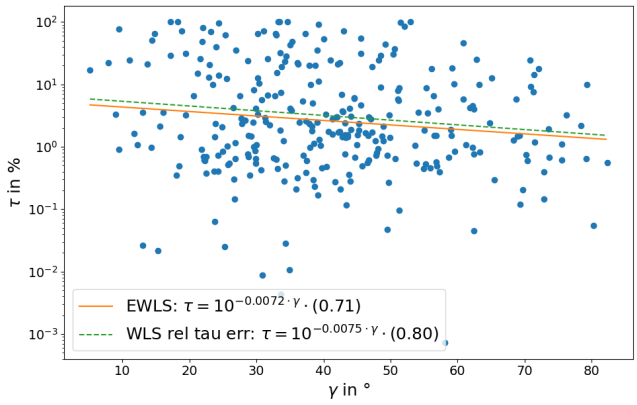

Fig. 10. Luminous efficiencies as derived in this work plotted over the event's entry angle γ with a fit through the data in semi-log space. Blue dots: values of τ. Orange line: equal-weighted least-squares fit (EWLS) applied to the data. Green dashed line: weighted least-squares fit (WLS) applied to the data; the method weights the values by the relative error of the value.

The luminous efficiency values derived in this study are about two orders of magnitude larger than the values published in the works of Subasinghe & Campbell-Brown (2018) and Čapek et al. (2019) but show a similar dependency on the meteoroids' masses. It should be mentioned that in both those works, only 15 (respectively 53), and especially smaller objects (10^{-6}–10^{-4} kg), were analysed. Nonetheless, the FRIPON data also include some meteoroids in the same size range.

The similar slope of all fits, indicating a weak relationship between the luminous efficiency and the initial meteoroid mass with negative linear behaviour in log–log space in combination with different y-axis intersections, could point towards a systematic error in the brightness determination and efficiency assumptions. A systematic bias due to different heights of the investigated objects based on their different masses could also influence the results and is an interesting aspect for future studies, as we demonstrate below.

For most of the events, the luminous efficiency values computed in this work are around one order of magnitude larger than the τ-values that are based on the photometric equations published in the literature. Depending on the results used for comparison, some luminous efficiencies differ by orders of magnitude. It has to be noted that the luminous efficiencies published in the literature, for which an overview is given in Table 1, also differ among themselves by orders of magnitude.

Interestingly, the asteroid studies found somewhat larger values for τ of the order of a few tens of percent. However, our data indicate that the luminous efficiency decreases with increasing mass. The correlation between the angle of entry and τ was also based on studies of particularly large objects, and the FRIPON data did only show a rather weak relation.

Nonetheless, to quantify the relation between the luminous efficiency and the entry angle of the events, a least-squares fit was used to optimise the parameters of the function $\tau = \eta \cdot 10^{\zeta \cdot \gamma}$. This is presented in Fig. 10 in semi-log space. EWLS gave $\zeta = -0.0072 \pm 0.0031$ and $\eta = 0.71 \pm 0.14$, WLS $\zeta = -0.0075 \pm 0.0032$, and $\eta = 0.80 \pm 0.14$. We expect the WLS method to represent the best estimate:

$$\tau = 0.80 \times 10^{-0.0075 \cdot \gamma}. \quad (13)$$

Even if the slightly negative slope agrees with the work by Svetsov & Shuvalov (2018), since they found that objects with very shallow angles especially show large luminous efficiencies, we advise not overestimating this weak link and to keep a rather large scattering in mind.

6. Uncertainties and model limitations

The new results presented are all based on data from the FRIPON fireball network. Recorded events are naturally of differing quality. To account for this, at least to some extent, less than ten percent of the available FRIPON events are used. The selection is based on the quality of the recorded data. This leads to our sample of the 294 most reliable events used for the derivation of the luminous efficiency. The data presented in the sections above always include results for this complete data set.

In the results of the derived properties, a visible scattering can be seen. This can be expected for a physically diverse set of meteors. In addition, some of the derived properties, and especially the luminous efficiency, have values that are clearly unphysical and unrealistic. To better understand this behaviour, several sources of uncertainty and errors are possible.

An important source of uncertainties are the investigated light curves themselves. So far, the brightness values are extracted from the single-station data, which are averaged and cleaned for outliers. It could be discussed if the method is sufficient or if, for example, a station weighting by quality should be taken into account, similar to the approach Jeanne et al. (2019) carried out for their astrometric data reduction. This could improve the quality of the light curves used as input for the analysis. However, we do not think that this would lead to a significant change in our results. We expect the present method to be a good compromise between accuracy and computational effort due to the relative low resolution of all-sky camera data.

An important factor to influence the brightness and light curve of a meteor is fragmentation. The method used in this work to obtain the luminous efficiency is based on the ablation and deceleration of the meteors. Fragmentation was not taken into account during this study. The role of fragmentation was, for example, demonstrated in a study of the ablation of two very bright bolides (Borovička & Spurný 1996). Larger values of τ for fragmenting objects were also found, for example,

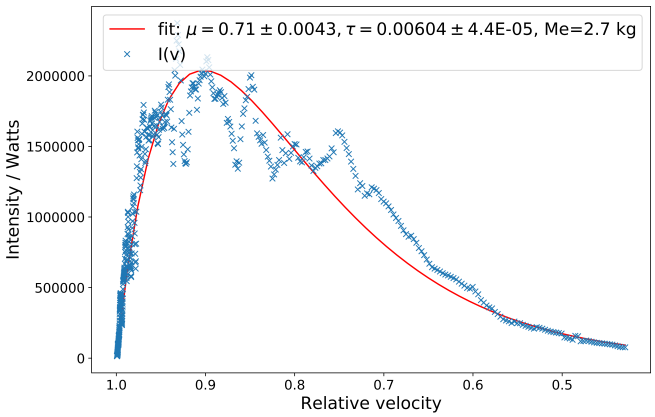

Fig. 11. Computed light curve with an applied fit. The light curve is from a fireball recorded on 05 October 2016 and shows a clear fragmentation (legend as in Fig. 3).

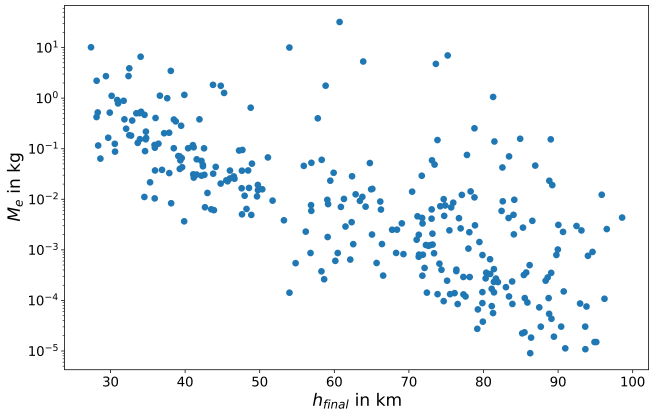

Fig. 12. Pre-atmospheric mass M_e of the entering object over its end height h_{final}.

by Subasinghe & Campbell-Brown (2018). For their investigated fragmenting meteoroids, the luminous efficiencies increased from less than 1% for most of their analysed meteors to τ-values up to a few tens of percent.

As found by Ceplecha & ReVelle (2005), for example, fragmentation could introduce large errors in the derived values of the luminous efficiencies and shift them towards much higher values. In their study, they confirmed that the reason for the 'historical' discrepancy of meteoroid masses determined from deceleration ('dynamic mass') and from brightness ('photometric mass') is meteoroid fragmentation. They argued that the deceleration-based method only measures the mass of the largest fragment and that the brightness is computed from the sum of the contributions of all fragments and dust particles. Hence, either these two masses or the luminous efficiencies differ for the photometric- and deceleration-based method. The negative dependency of the luminous efficiency on the pre-atmospheric mass obtained in this study and found by Subasinghe & Campbell-Brown (2018) and Čapek et al. (2019) could probably be a bias caused by fragmentation. It is possible that the more severe the fragmentation is, the lower the (smaller) dynamic mass is, and hence the higher the luminous efficiency. This could cause a shift in the $\tau - M_e$ diagram towards the upper left of strong fragmenting objects, and a shift towards the lower right of objects with less fragmentation.

How much influence this possible bias has could be part of future work, and since most meteoroids fragment as shown by Subasinghe et al. (2016), for example, we do expect a similar behaviour for the objects in the investigated data set of FRIPON meteors. We do expect most of our analysed events to fragment at least to some degree. Some light curves show clear signs of fragmentation. Figure 11 gives one example with clearly visible spikes, which could be attributed to fragmentation events. Nonetheless, these events were also used if the fit for μ and τ appeared reasonably accurate.

In principle, observed fragmentations could and would be an interesting parameter to be considered. However, this would introduce new parameters and uncertainties. It would also give the total or maximum photometric brightness, which could be dominated by the total number of fragments and the assumption of a luminous efficiency might lose its meaning. If high-resolution recordings (in time and space) are available, it might be possible to derive the light curve based on the fragmentations, but the result would only apply for one specific event.

Other uncertainties are introduced by the assumptions of values for the computations of the drag coefficient c_d, the pre-atmospheric shape factor of the meteoroid A_e, and the meteoroid bulk density ρ. They can affect the results significantly. As mentioned before, assumptions for these values vary a lot depending on the studies. In the presented method, a lower bulk density of the source object should reduce the derived luminous efficiency. This effect is being analysed in ongoing work. The analysed sample of meteoroids consists of sporadic and stream objects that certainly have differing bulk densities, which in many cases are lower than the constant value of 2500 kg m^{-3} used in this study.

Finally, the method itself should be investigated for possible error sources. Since the method is based on the analysis of deceleration data, it is expected to be most robust for larger events with low end heights for which the deceleration is very prominent in the data. Figure 12 presents the mass of the entering object over its end height, h_{final}. As expected, larger objects have considerably lower end heights.

The low number of small and fast events with larger end heights can be explained by the following physical factors. According to the method used in this work, small objects would only be detected if a large part of their energy were converted into visible light or if they fragmented heavily, thus increasing their brightness. This leads to an observational bias that should be taken into consideration. It is suspected that the ablation-based method used in this study is not entirely applicable for some of the recorded events. This could explain the unrealistically high luminous efficiency values for some events.

Visible objects that decelerate over longer time periods will usually penetrate the atmosphere deeper. Such objects seem the best candidates to match the assumptions of the present deceleration-based method. These objects could show only little fragmentation allowing the major body to ablate continuously in line with the model. To support this idea, we studied a sample of events reaching deeper into the atmosphere as determined by its final height.

Particularly low penetrating events with final heights under 55 km make up a subset of about 40% of our complete data set.

Figure 13 shows the distribution of τ over the pre-atmospheric mass of the object. It shows the same as Fig. 9 but only for the events with end heights, h_{final}, below 55 km, representing a subset of 115 objects. It can be seen that the smallest meteoroids were excluded this way and that the luminous efficiency values in Fig. 13 are smaller than the ones in Fig. 9. This was expected since smaller objects tend to have higher end

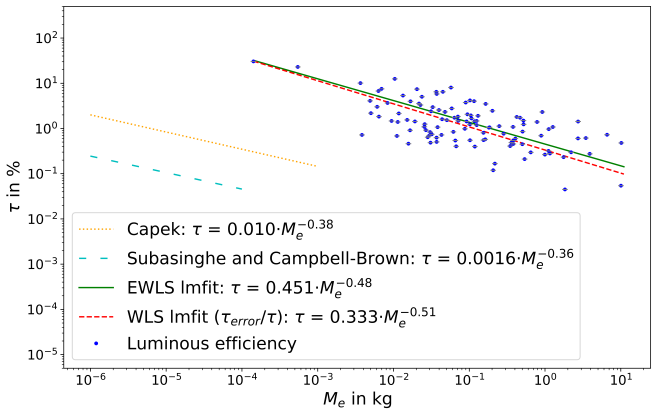

Fig. 13. Same as Fig. 9, but only for the 115 events with an end height below 55 km.

heights (compare to Fig. 12) and the previously established trend towards larger τ-values for smaller entry masses. The result of the WLS for this low-end-height subset is shown in Eq. (14). The fit has a slightly smaller shift but a steeper slope than the fit through all the investigated events (compare Eq. (12)):

$$\tau = 0.33 \cdot M_{\rm e}^{-0.51}. \quad (14)$$

The degree of deeper atmospheric penetration is likely also associated with a higher tensile strength that informs us about the transition between fluffy cometary aggregates and rocky chondritic meteoroids (Blum et al. 2006, 2014; Trigo-Rodríguez & Blum 2009; Beitz et al. 2016; Vernazza et al. 2015). Since larger meteoroids with higher tensile strength are able to penetrate the atmosphere deeper, most events with low initial masses and of fluffy cometary nature are not included in this subset. Additionally, we expect the events with low end heights and large masses to be the most suitable ones for analysis with our method, and thus we assume a rather high quality of results in those cases. The luminous efficiency values for the larger masses have not changed significantly from those obtained for the full sample (compare to Fig. 9), but the physically unrealistic values have disappeared. The subset of events shown in Fig. 13 need not be the only one for which the present ablation-based method works, but we expect reliable τ calculations for these events.

In ongoing work, additional biases, the range of applicability of the present method, and the dependency of the luminous efficiency on various model parameters are further investigated.

7. Conclusions

One of the most important and controversially discussed meteor parameters for the conversion from magnitude to mass is the luminous efficiency τ. In the course of this work, the data of the FRIPON optical video camera system was used, and a robust calculation method for the luminous efficiency was applied. We calculated the luminous efficiencies of meteors and fireballs using deceleration-based formulas and compared our results to values published in the literature. Luminous efficiencies and shape change coefficients were determined for a total of 294 events with computed pre-atmospheric meteoroid masses in the 10^{-6}–10^{2} kg range. These 294 events were selected from a sample of more than 3000 FRIPON events based on the quality of the data. Preliminary results were obtained from an initial analysis based on all 294 events.

We are able to confirm a dependency of τ on the velocity of the event in the investigated data. The relation $\tau = 0.0023 \cdot v_{\rm e}^{2.3}$ was found. As expected, this implies that the radiation of faster meteoroids is more efficient. It could be explained as a consequence of higher excitation potentials and by the presence of a second spectral component of high temperature exhibiting important emission lines in the optical range. Moreover, a relationship between the luminous efficiency and the initial meteoroid mass with negative linear behaviour was found: $\tau = 0.48 \cdot M_{\rm e}^{-0.47}$. This points to the fact that smaller meteoroids radiate more efficiently. The correlation between the angle of entry and τ did only show a weak dependency of: $\tau = 0.80 \cdot 10^{-0.0075 \cdot \gamma}$.

Although the luminous efficiency values derived in this work range from 10^{-4}–100%, most of them are of the order of 0.1–10%. This is considerably larger than in most meteor studies, especially for smaller objects, but it is well within the range found in studies of fireballs and larger asteroids. The dependency of τ on the meteoroid's mass with a slightly negative slope agrees with more recent studies.

By careful analysis of the calculated luminous efficiencies and cross-correlations with several parameters, we realised that the ablation-based method has certain limitations. In some cases, especially for small meteoroids and those with short deceleration durations unrealistically high values for the luminous efficiency were obtained. The assumption of a smooth ablation and deceleration seems to break down in certain cases. The neglect of fragmentation probably has the biggest impact. Fragmentation was observed in many of the analysed events. A detailed analysis of fragmentation would likely require dedicated observations with very high spatial and time resolutions. Consideration of fragmentation would also lead to another parameter with additional uncertainties and assumptions that could be challenged. In addition, each fragmentation event would be different, and a derived luminous efficiency would likely only be valid for that specific event. Moreover, it should also be mentioned that we only calculated one constant value for τ for each event. The fact that the luminous efficiency can change in the course of the meteor phenomenon is not taken into account.

In our study, we concentrated on understanding the biases, advantages, and shortcomings of the method used. For an initial hint of the range of applicability of the ablation-based model, we looked at a subset of events that penetrated to 55 km altitude or below. Typically, these objects also have longer periods of recorded deceleration values. We believe that these events are most compatible with our model assumptions. Most of the source objects of the qualifying 115 events have calculated initial masses in the 0.005 kg to 10 kg range. For the luminous efficiency as a function of mass, the relation $\tau = 0.33 \cdot M_{\rm e}^{-0.51}$ was found (with initial mass $M_{\rm e}$ in kg). Unphysical luminous efficiency values no longer appear in this data set. We believe that the calculated luminous efficiency values for this data set are quite reliable.

The obtained relationship between the luminous efficiency and the initial meteoroid mass shows a negative behaviour. In our study, this trend is found for the complete data set and for the reduced set with larger and deeper penetrating objects. This agrees with the results of previous studies for smaller source particles. Several explanations for this finding seem possible. Smaller objects might only be visible if they have truly a higher luminous efficiency. It could also be that smaller objects only become visible if they fragment heavily, which increases their luminosity, or that this is the result of a smaller surface-to-volume ratio for larger objects, which leads to a reduced

luminous efficiency because of a relatively smaller ablation area. Many interesting aspects are still open for future interpretation and analysis. Future work might entail the study of more FRIPON data, using only the highest quality FRIPON data, or taking into account the shower affiliation of the events. A study of the effect of different bulk densities on the luminous efficiency is ongoing.

A comparison of the obtained results with results based on data from other sensors or applying another method to determine the luminous efficiency to the FRIPON data could also be an interesting feature of future works. A more detailed analysis of the range of applicability of the deceleration method is in progress. That study will also assess additional correlations of meteor parameters and investigate the dependence of the luminous efficiency on the bulk density of the source object. The wealth of data from the large FRIPON network will certainly provide new insights into the meteoroid environment and its interaction with the Earth's atmosphere.

Acknowledgements. We thank the European Space Agency and the University of Oldenburg for funding this project. We would especially like to thank Maria Gritsevich for her support and constructive discussions on this matter. A special gratitude goes to the FRIPON Network for providing the data used for this study and to the FRIPON team for their support of this project. All the data used in the present publication were obtained and made available by the FRIPON network (www.fripon.org). FRIPON was initiated by funding from ANR (grant no. 13-BS05-0009-03), carried by the Paris Observatory, Muséum National d'Histoire Naturelle, Paris-Saclay University and Institut Pythéas (LAM-CEREGE). VigieCiel was part of the 65 million d'Observateurs project, carried by the Muséum National d'Histoire Naturelle and funded by the French Investissements d'Avenir program. FRIPON data are hosted and processed at Institut Pythéas SIP (Service Informatique Pythéas), and a mirror is hosted at IMCCE (Institut de Mécanique Céleste et de Calcul des Éphémérides/Paris Observatory) with the help of IDOC8 (Integrated Data and Operation Center), supported by CNRS and CNES. PRISMA is the Italian Network for Systematic surveillance of Meteors and Atmosphere. It is a collaboration initiated and coordinated by the Italian National Institute for Astrophysics (INAF) that counts members among research institutes, universities, associations and schools. The complete list of PRISMA members is available here: http://www.prisma.inaf.it. PRISMA was funded by 2016/0476 and 2019/0672 Research and Education grants from Fondazione Cassa di Risparmio di Torino and by a 2016 grant from Fondazione Agostino De Mari (Savona). FRIPON-Spain is coordinated from the Institute of Space Sciences (CSIC-IEEC). J.M.T.-R. and E.P.A. acknowledge financial support from the Spanish Ministry (PGC2018-097374-B-I00, PI: J.M.T.-R.). We were additionally supported by the J.M.T.-R. research project PGC2018-097374-B-I00 funded by MCI-AEI-FEDER, EU.

References

Anghel, S., Birlan, M., Nedelcu, D.-A., & Boaca, I. 2019, Romanian Astron. J., 29, 3
Audureau Y., Marmo C., Bouley S., et al. 2014, Proceedings of the International Meteor Conference 2014, eds. J.-L. Rault, & P. Roggemans, 39
Ayers, W. G., McCrosky, R. E., & Shao, C.-Y. 1970, SAO Special Report #317
Beitz E., Blum, J., Parisi, M. G., & Trigo-Rodríguez, J. M. 2016, ApJ, 824, 12
Blum, J., Schräpler, R., Davidsson, B. J. R., & Trigo-Rodríguez, J. M. 2006, ApJ, 652, 1768
Blum, J., Gundlach, B., Muhle, S., & Trigo-Rodríguez, J. M. 2014, Icarus, 235, 156
Borovička, J. 1993, A&A, 279, 615
Borovička, J. 1994, PSS, 42, 145
Borovička, J., & Spurný, P. 1996, Icarus, 121, 153
Borovička, J., Stork, R., & Bocek, J. 1999, MAPS, 34, 987
Brown, P., Assink, J., Astiz, L., et al. 2013, Nature, 503, 235
Brownlee, P., Tsou, P., Aléon, J., et al. 2006, Science, 314, 1711
Campbell-Brown, M. D., & Koschny, D. 2004, A&A, 418, 2
Campbell-Brown, M. D., Kero, J., Szasz, C., & Pellinen-Wannberg, A. 2012, J. Geophys. Res., 117, A09323
Čapek, D., Koten, P., Borovička, J., et al. 2019, A&A, 625, A106
Ceplecha, Z., & McCrosky, R. E. 1976, J. Geophys. Res., 81, 35
Ceplecha, Z., & ReVellle, D. O. 2005, MAPS, 40, 1
Ceplecha, Z., Borovicka, J., Elford, W. G., et al. 1998, Space Sci. Rev., 84, 3/4
Colas, F., Zanda, B., Bouley, S., et al. 2014, Proceedings of the International Meteor Conference 2014, eds. J.-L. Rault, & P. Roggemans, 34
Colas, F., Zanda, B., Bouley, S. et al. 2020, A&A, 644, A53
Devillepoix, H., Cupák, M., Bland, P., et al. 2020, PSS, 191, 105036
Drolshagen, S., & Kretschmer, J. 2015, Bachelor thesis (University of Oldenburg)
Drolshagen, E., & Ott, T. 2014, Bachelor thesis (University of Oldenburg)
ECSS, European Cooperation for Space Standardization 2008, Space Engineering, Space Environment, ECSS-E-ST-10-04C
Everitt, B. S., & Skrondal, A. 2002, The Cambridge Dictionary of Statistics (New York: Cambridge University Press)
Friichtenicht, J. F., Slattery, J. C., & Tagliaferri, E. 1968, NASA, CR-787
Gardiol, D., Cellino, A., & Di Martino, M. 2016, Int. Meteor Conf. 2016, 76
Gardiol, D., Affaticati, F., Albani, M., et al. 2019, Proceedings of the International Meteor Conference 2018, 81
Gómez-Martín, J. C., Bones, D. L., Carrillo-Sánchez, J. D., et al. 2017, ApJ, 836, 212
Gritsevich, M. 2008a, Dokl. Phys., 53, 2
Gritsevich, M. I. 2008b, Solar Syst. Res. 42, 5
Gritsevich, M., & Koschny, D. 2011, Icarus, 212, 2
Gritsevich, M., Lyytinen, E., Moilanen, J., et al. 2014a, Proceedings of the International Meteor Conference 2014, 162
Gritsevich, M., Lyytinen, E., Kohout, T., et al. 2014b, MAPS, 49, A143
Halliday, I. Griffin, A. A., & Blackwell, A. T. 1981, Meteoritics, 16, 2
Halliday, I., Griffin, A. A., & Blackwell, A. T. 1996, MAPS, 31, 185
Howie, M., Paxman, J., Bland, P. A., et al. 2017, Exp. Astron., 43, 237
Hill, K. A., Rogers, L. A., & Hawkes, R. L. 2005, A&A, 444, 615
IMO 2015, International Meteor Organization, (1997–2013 International Meteor Organization) [online]
IMO 2017, International Meteor Organisation – 2018 Meteor Shower, ed. R. Calendar
Jeanne, S., Colas, F., Zanda, B., et al. 2019, A&A, 627, A78
Jones, W., & Halliday, I. 2001, MNRAS, 320, 4
Koschny, D., Bettonvil, F., Licandro, J., et al. 2013, Geosci. Instrum. Methods Data Syst., 2, 189
Koschny, D., Drolshagen, E., Drolshagen, S., et al. 2017, PSS, 143, 256
Moreno-Ibáñez, M., Silber, E. A., Gritsevich, M., & Trigo-Rodríguez, J. M. 2018, ApJ, 863, 174
Moreno-Ibáñez, M., Gritsevich, M., Silber, E. A., & Trigo-Rodriguez, J. M. 2020, MNRAS, staa646
Nedelcu, D. A., Birlan, M., Turcu, V., et al. 2018, Roman. Astron. J., 28, 1
Nemtchinov, I. V., Svetsov, V. V., Kosarev, I. B., et al. 1997, Icarus, 130, 2
Oberst J., Molau, S., Heinlein, D., et al. 1998, MAPS, 33, 49
Ott, T., Drolshagen, E., Koschny, D., et al. 2020, Acta Astronaut., 177, 172
Rietmeijer, F. J. M. 2004, EPS, 95, 321
Sansom, E. K., Gritsevich, M., Devillepoix, H. A. R., et al. 2019, ApJ, 885, 115
Sosa, A., & Fernández, J. A. 2009, MNRAS, 393, 1
Stulov, V. P., Mirskii, V. N., & Vislyi, A. I. 1995, Aerodinamika bolidov (Aerodynamics of Bolides) (Moscow, Russia: Nauka)
Subasinghe, D., & Campbell-Brown, M. 2018, ApJ, 155, 88
Subasinghe, D., Campbell-Brown, M. D., & Stokan, E. 2016, MNRAS, 457, 1289
Subasinghe, D., Campbell-Brown, M., & Stokan, E. 2017, PSS, 143, 71
Svetsov, V. V., & Shuvalov, V. V. 2018, Earth Planet. Sci. Lett., 503, 10
Svetsov, V. V., & Shuvalov, V. V. 2019, MAPS, 54, 126
Svettsov, V. V., Shuvalov, V. V., & Popova O. P. 2018, Solar Syst. Res., 52, 195
Toth, J., Kornos, L., Piffl, R., et al. 2012, Proceedings of the International Meteor Conference 2011, 82
Trigo-Rodríguez, J. M. 2019, Hypersonic Meteoroid Entry Physics, ed. Colonna G., Capitelli M., & Laricchiuta A. (Institute of Physics Publishing), 4
Trigo-Rodríguez, J. M., & Blum, J. 2009, PSS, 57, 243
Trigo-Rodríguez, J. M., & Llorca, J. 2006, MNRAS, 372, 655
Trigo-Rodríguez, J. M., & Llorca, J. 2007, MNRAS, 375, 415
Trigo-Rodríguez, J. M., Llorca, J., Borovicka, J., & Fabregat, J. 2003, MAPS, 38, 1283
Trigo-Rodríguez, J. M., Castro-Tirado, A., Llorca, J., et al. 2004, EPS, 95, 375
Trigo-Rodríguez, J. M., Llorca, J., Castro-Tirado, A. J. et al. 2006, Astron. & Geophys., 47, 6
Trigo-Rodríguez, J. M., Domínguez, G., Burchell, M. J., Hörz, F., & Llorca, J. 2008, MAPS, 43, 23
Trigo-Rodríguez, J. M., Madiedo, J. M., Williams, I. P., et al. 2013, MNRAS, 433, 560
Trigo-Rodríguez, J. M., Rimola, A., Tanbakouei, S., Cabedo-Soto, V., & Lee, M. R. 2019, Space Sci. Rev., 215, 18
Vernazza, P., Marsset, M., Beck, P., et al. 2015, ApJ, 806, 204
Verniani, F., 1965, Smithsonian Contri. Astrophys., 8, 141
Weryk, R. J., & Brown, P. G. 2013, PSS, 81, 32
Weryk, R. J., Campbell-Brown, M. D., Wiegert, P. A., et al. 2013, Icarus, 225, 1

[1] University of Oldenburg, Division for Medical Radiation Physics and Space Environment, Germany
e-mail: esther.drolshagen@uni-oldenburg.de; theresa.ott@uni-oldenburg.de
[2] European Space Agency, ESTEC, Keplerlaan 1, 2201 AZ Noordwijk, The Netherlands
[3] Chair of Astronautics, TU Munich, Germany
[4] IMCCE, Observatoire de Paris, PSL Research University, CNRS UMR 8028, Sorbonne Université, France
[5] Institut de Minéralogie, Physique des Matériaux et Cosmochimie (IMPMC), Muséum National d'Histoire Naturelle, CNRS UMR 7590, Sorbonne Université, 75005 Paris, France
[6] FRIPON (Fireball Recovery and InterPlanetary Observation) and Vigie-Ciel Team, France
[7] GEOPS-Géosciences, CNRS, Université Paris-Saclay, 91405, Orsay, France
[8] Service Informatique Pythéas (SIP) CNRS - OSU Institut Pythéas – UMS 3470, Marseille, France
[9] Aix Marseille Univ, CNRS, CNES, LAM, Marseille, France
[10] INAF - Osservatorio Astrofisico di Torino - Via Osservatorio 20, 10025 Pino Torinese, TO, Italy
[11] Astronomical Institute of the Romanian Academy, Bucharest, 040557, Romania
[12] MOROI (Meteorites Orbits Reconstruction by Optical Imaging) Astronomical Institute of the Romanian Academy, Bucharest, Romania
[13] SCAMP (System for Capture of Asteroid and Meteorite Paths), FRIPON, UK
[14] Planétarium Rio Tinto Alcan/Espace pour la vie, Montréal, Québec, Canada
[15] Réseau DOME, (Détection et Observation de Météores/Detection and Observation of Meteors), Canada
[16] SPMN (SPanish Meteor Network), FRIPON, Spain
[17] Institute of Space Sciences (CSIC), Campus UAB, Facultat de Ciències, 08193 Bellaterra, Barcelona, Catalonia, Spain
[18] Institut d'Estudis Espacials de Catalunya (IEEC), 08034 Barcelona, Catalonia, Spain
[19] FRIPON-Belgium.
[20] Royal Belgian Institute for Space Aeronomy, Brussels, Belgium
[21] Natural History Museum, Burgring 7, 1010 Vienna, Austria
[22] FRIPON-Austria.
[23] Università degli Studi di Torino, Dipartimento di Fisica, Via Pietro Giuria 1, 10125 Torino, TO, Italy
[24] INAF – Osservatorio di Astrofisica e Scienza dello Spazio Via Piero Gobetti 93/3, 40129 Bologna, BO, Italy
[25] INAF – Istituto di Astrofisica e Planetologia Spaziali Via del Fosso del Cavaliere 100, 00133 Roma, RM, Italy
[26] CNR – Istituto di Fisica Applicata Nello Carrara, Via Madonna del Piano 10, 50019 Sesto Fiorentino (FI), Italy
[27] Space sciences, Technologies Astrophysics Research (STAR) Institute, Université de Liège, Liège 4000, Belgium
[28] Universitat degli Studi di Firenze - Dipartimento di Scienze della Terra, Via Giorgio La Pira, 4, 50121 Firenze, FI, Italy
[29] Natural History Museum, Cromwell Road, London, UK
[30] Dep. Fisica Aplicada I, Escuela de Ingeniera de Bilbao, Universidad del Pais Vasco/Euskal Herriko Unibertsitatea, 48013 Bilbao, Spain
[31] Aula EspaZio Gela, Escuela de Ingeniera de Bilbao, Universidad del Pais Vasco/Euskal Herriko Unibertsitatea, 48013 Bilbao, Spain
[32] FRIPON-Netherlands, European Space Agency, SCI-SC, Keplerlaan 1, 2201 AZ Noordwijk, The Netherlands
[33] Osservatorio Astronomico del Righi, Via Mura delle Chiappe 44R, 16136 Genova, GE, Italy
[34] Departament de Quimica, Universitat Autonoma de Barcelona, 08193 Bellaterra, Catalonia, Spain

Appendix A: Deceleration-based computations

Based on the drag and mass loss equations, Gritsevich (2008a) derived a formula dependent on the dimensionless parameters α and β, as well as on the dimensionless velocity v^* (see Eq. (7) in Gritsevich 2008a, Eq. (A.2)). This equation represents a height-velocity relation for which α and β represent the best solution. Since v^* depends only on the deceleration of the meteoroid, it is possible to determine the proper values of α and β obtained from the best least-squares fit of the observed heights and velocities for Eq. (A.2).

This method has the main advantage that no assumptions of the meteoroids' parameters have to be made. The parameters α and β can be derived by using only the (generally accurately measurable) altitude of the meteoroid and its velocity:

$$m^* = \exp\left(-\beta \cdot \frac{1 - v^{*2}}{1 - \mu}\right), \tag{A.1}$$

$$y^* = \ln(\alpha) + \beta - \ln\left(\frac{\overline{Ei}(\beta) - \overline{Ei}(\beta \cdot v^{*2})}{2}\right), \tag{A.2}$$

with the following dimensionless mass and height:

$$m^* = \frac{M}{M_e},\ y^* = \frac{h}{h_0}. \tag{A.3}$$

Appendix B: Data, results, and discussion

In Fig. B.1, τ as a function of μ with fitting errors for both values can be seen. Figure B.2 presents the luminous efficiencies plotted over the events' velocities, Fig. B.3 shows τ over the events' corresponding meteoroids' masses, and Fig. B.4 presents τ over the events' entry angles γ.

Halliday et al. (1996) derived a relationship for τ (with v in km s^{-1}) as given in Eqs. (B.1) and (B.2):

$$\tau_{Halliday\ et\ al.} = 0.04, \qquad v < 36\,\mathrm{km\,s^{-1}}, \tag{B.1}$$

$$\tau_{Halliday\ et\ al.} = 0.069 \cdot \left(\frac{36}{v}\right)^2, \qquad v \geq 36\,\mathrm{km\,s^{-1}}. \tag{B.2}$$

Ceplecha & McCrosky (1976) published a dependency of the luminous efficiency on the fireball velocity as presented in Eqs. (B.3)–(B.7):

$$\log(\tau_{Ceplecha\&McCrosky}) = -12.75, \qquad v < 9.3\,\mathrm{km\,s^{-1}} \tag{B.3}$$

$$\log(\tau_{Ceplecha\&McCrosky}) = -15.6 + 2.92 \cdot \log(v), \qquad 9.3\,\mathrm{km\,s^{-1}} < v < 12.5\,\mathrm{km\,s^{-1}} \tag{B.4}$$

$$\log(\tau_{Ceplecha\&McCrosky}) = -13.24 + 0.77 \cdot \log(v), \qquad 12.5\,\mathrm{km\,s^{-1}} < v < 17.0\,\mathrm{km\,s^{-1}} \tag{B.5}$$

$$\log(\tau_{Ceplecha\&McCrosky}) = -12.5 + 0.17 \cdot \log(v), \qquad 17.0\,\mathrm{km\,s^{-1}} < v < 27.0\,\mathrm{km\,s^{-1}} \tag{B.6}$$

$$\log(\tau_{Ceplecha\&McCrosky}) = -13.69 + \log(v), \qquad 27.0\,\mathrm{km\,s^{-1}} < v < 72.0\,\mathrm{km\,s^{-1}}. \tag{B.7}$$

Converted to the formalism used in this work, Subasinghe & Campbell-Brown (2018) found a relation between τ and the pre-atmospheric meteoroid's mass M_e as given in Eq. (B.8). Čapek et al. (2019) found a similar relation. Converted for masses in kg, it would be expressed as stated in Eq. (B.9):

$$\tau_{Subasinghe\&Campbell-Brown} = 0.0016 \cdot M_e^{-0.3647}, \tag{B.8}$$

and for masses in kg,

$$\tau_{Capek\ et\ al.} = 0.01 \cdot M_e^{-0.38}. \tag{B.9}$$

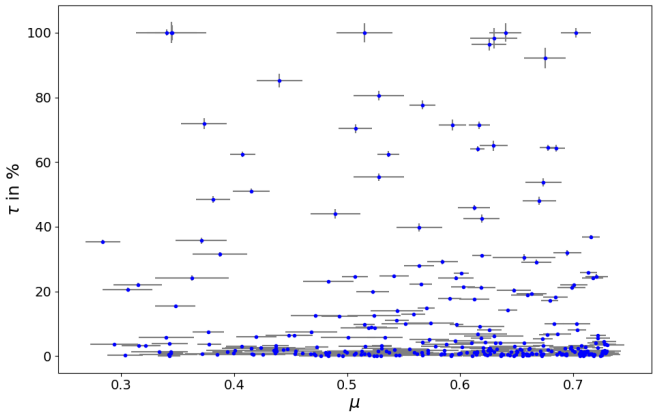

Fig. B.1. τ as a function of μ with fitting errors for both values.

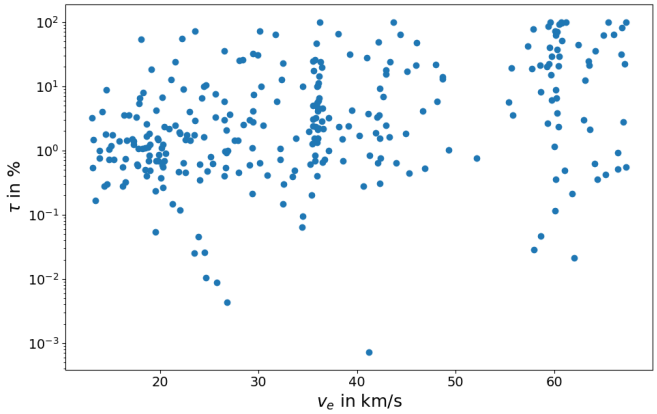

Fig. B.2. Luminous efficiencies τ over the events' pre-atmospheric velocities v_e in semi-log space.

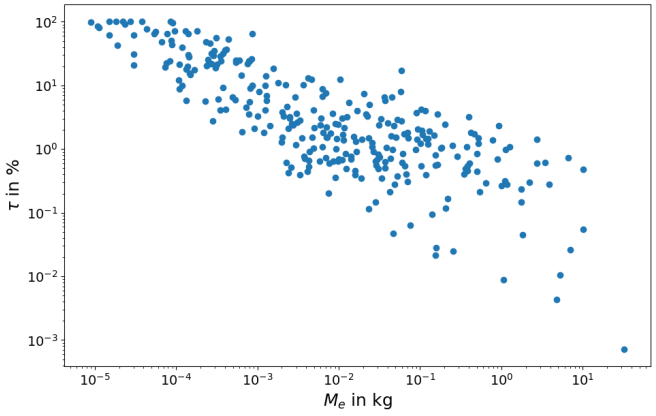

Fig. B.3. Luminous efficiency τ over the events' corresponding pre-atmospheric meteoroid masses M_e in log–log space.

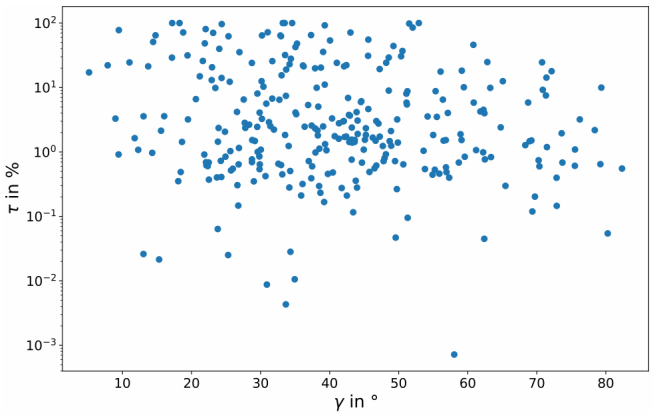

Fig. B.4. Luminous efficiency τ over the events' entry angles γ in semi-log space. The entry angle is measured from the horizon.